MAPPING THE LUNAR PHASE FUNCTION IN THE NEAR-INFRARED WITH THE LUNAR ORBITER LASER ALTIMETER. M. K. Barker[1], X. Sun[2], E. Mazarico[2], G. A. Neumann[2], D. E. Smith[2,3] and M. T. Zuber[3] [1]Sigma Space Corp., 4600 Forbes Blvd. Lanham, MD 20706 michael.barker@sigmaspace.com, [2]Solar System Exploration Division, NASA Goddard Space Flight Center 8800 Greenbelt Rd. Greenbelt, MD 20771, [3]Dept. of Earth, Atmospheric and Planetary Sciences, MIT, 77 Massachusetts Ave. Cambridge, MA 02139.

Introduction: The lunar phase function is of interest because it can yield information on the chemical and physical properties of the regolith, as well as surface processes like space weathering. Spatial variations in the lunar phase function have been found that are correlated with geologic context, most notably between the maria and highlands [1,2,3], but also at other locations with special geologic features, such as the Reiner Gamma Formation [1,4,5] and pyroclastic deposits [6]. Several studies have used phase ratio images, the ratio between two images of the same location taken at different phase angles, to infer aspects of the physical structure of the regolith, like the surface roughness or porosity [4,5].

In this study, we describe results on the measurement of the near-infrared phase function observed with the Lunar Orbiter Laser Altimeter (LOLA) onboard the Lunar Reconnaissance Orbiter. The unique capability of LOLA to passively measure reflected sunlight and also actively measure the normal albedo from the backscattered laser pulse energies allows a more robust estimation of the phase function than is typically possible with passive imagers.

Data: LOLA measures surface reflectivity at 1064 nm with two methods: (1) active radiometry and (2) passive radiometry. In method (1), the ratio of the backscattered and transmitted laser pulse energies yields the surface reflectivity at zero phase, called the normal albedo A_n, which is independent of topography. A global 4 pixel-per-degree (ppd) map of the LOLA 1064 nm A_n was recently produced and analyzed [7,8]. In method (2), the Sun is the light source and LOLA measures the number of solar photons reflected off the lunar surface into the detector. LOLA has been collecting passive radiometry in the northern hemisphere since December, 2013.

In its passive radiometry mode, LOLA acts as a 4-pixel radiometer with pixel size ~60 m and integration time of 1/28th sec (every ~60 m along-track). To boost the SNR, we use 5-exposure (0.18-sec) moving averages of Channels 2 - 5. With this 20-point averaging and ~4,200 orbits through the end of 2014, the total number of data points is ~200 million. The mean SNR of the averaged data points ranges from ~300 at the equator to ~25 at 85°N. We applied temperature-dependent dark current and responsivity corrections to each channel separately. The transformation from dark-subtracted, normalized counts to absolute radiance was estimated by matching ~2700 points in our dataset to nearby (< 1 km away) points in the SELENE Spectral Profiler dataset with similar viewing geometries [2].

Results: We calculate the phase function, first by dividing each point's radiance factor (RADF) by the Lommel-Seeliger limb-darkening law using the LOLA 128ppd global elevation model to derive the topography-dependent photometric angles. Then, we divided this value by the spatially resolved 1064 nm A_n map [8] to correct for surface reflectivity variation. This removes most of the effects of single-scattering particle albedo. Fig. 1 shows the resulting 1064-nm phase function for several different bins of FeO wt% for latitudes within 60° of the equator. The latter quantity was interpolated on the Clementine maps using the method of [9]. The maria and highlands form a continuous sequence of curves. This behavior is likely due to other parameters that are correlated with composition besides single-scattering albedo, such as the relative strength of backward and forward scattering in the single particle phase function, the opposition effect (OE) amplitude, and the OE width.

To look for spatial variations in the phase function besides those due to FeO, we made a color composite "phase difference" map (Fig. 2). This map shows the median difference between every point and the global phase function for that point's phase and FeO, bilinearly interpolated on the phase function grid of Fig. 1 in order to facilitate comparison between the

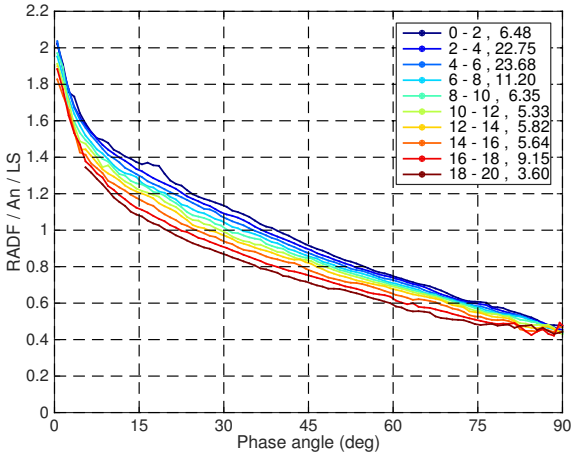

Figure 1 - The effect of FeO on the LOLA 1064-nm phase function color-coded by FeO wt%. The total number of data points included is ~120 million. The numbers after the commas in the legend give the percentage of data in each FeO bin.

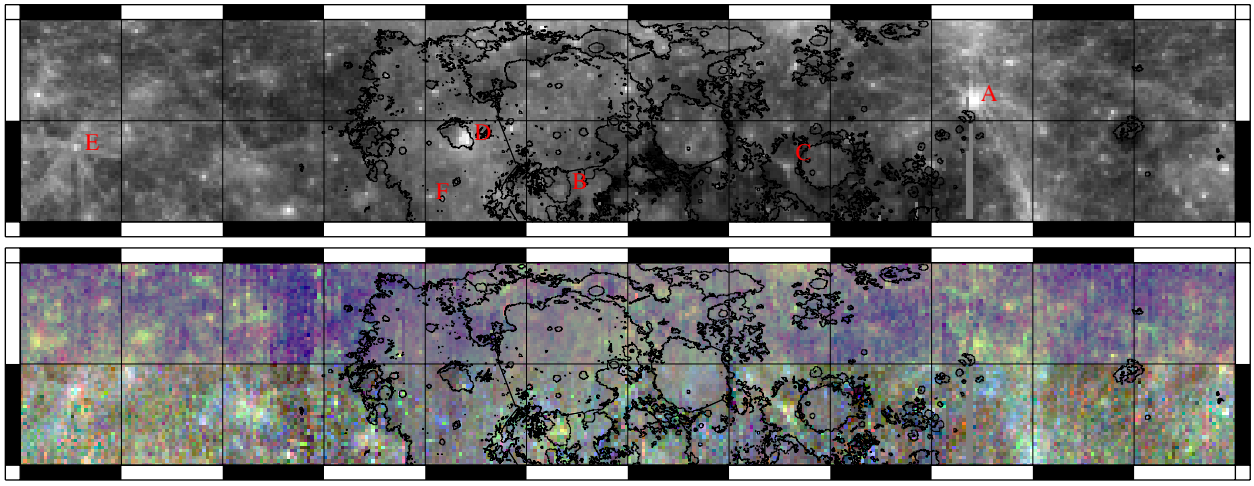

Figure 2 - Top panel: Optical maturity (OMAT) parameter based on Clementine UV-VIS imaging [10]. Map covers 0-60°N and is centered on 0°E. Grid lines are spaced every 30°. The maria are outlined with the shapefile of [11]. Bottom panel: Color composite phase difference map showing the median difference from an FeO-dependent median phase function (see text for details). Different phase angle ranges control the RGB color channels: 0-30° (blue), 30-60° (green), and 60-90° (red). The blue channel for latitudes > 30°N is set to a constant phase difference value of 0, causing only red and green hues there, due to the lack of data with phase < 30°.

maria and highlands. It is possible to identify spatially-localized deviations from the globally-typical phase function, which may be caused by real geologic variation. After removing the major FeO variations, the brightness and color variations in the phase difference map are generally correlated with variations in the OMAT map. Indeed, many of the most immature regions in the OMAT map are visible in the phase difference map as intensity enhancements. Above 30°N, the enhancements tend to be green or yellow because of the lack of data with phase < 30°. Several large, young craters and their immature ejecta are clearly visible in the phase difference map, such as Giordano Bruno, (A), Copernicus (B), Proclus (C), and Jackson (E). Jackson appears as a blue-green enhancement surrounded by pink pixels with an overall SW-NE orientation. Its bright ejecta are visible as slight purple enhancements extending out hundreds of km. This crater has a dark halo which is generally considered to be an impact melt deposit [12]. The dark halo has a spectral signature distinct from the surrounding ejecta as seen in a Clementine UV-VIS color-ratio composite image [13]. The pink pixels surrounding the crater in the phase difference map are approximately co-spatial with the dark halo deposit. The Aristarchus plateau (D), a region of known pyroclastic volcanism [14], does not have a significant enhancement in the phase difference map despite being one of the most prominent features in the OMAT map. The OMAT parameter could be overestimated in this region because it is not calibrated for pyroclastic glass. In addition, the different grain properties of the pyroclastic material may change the phase function relative to typical regolith with the same exposure age. The Reiner Gamma Formation (F) is one of the few enhancements in the maria, consistent with previous studies of its unusual photometric behavior [1,4,5].

Summary: In this work, we present just a sample of results from the passive radiometry collected by LOLA over the course of ~12 months during the LRO extended science mission phase 2. On a global scale, we find that iron abundance and optical maturity are the dominant controlling parameters of phase function shape. The phase difference map reveals additional geologically-influenced variations in the phase function. In future work we will examine the nature of these variations in more detail. Laser altimeters like LOLA can contribute to studies of planetary reflectance properties thanks to their combined active and passive radiometry measurements at all phase angles.

References: [1] Kreslavsky, M. A. et al. (2000) *JGR*, 105, 20281. [2] Yokota et al. (2011) *Icarus*, 215, 639. [3] Sato, H. et al. (2014) *JGR Plan.*, 119, 1775. [4] Kreslavsky, M. A. & Shkuratov, Y. G. (2003) *JGR Plan.*, 108, 5015. [5] Kaydash, V. et al. (2009) *Icarus*, 202, 393. [6] Souchon, A. L. et al. (2013) *Icarus*, 225, 1. [7] Lucey, P. et al. (2014) *JGR Plan.*, 119, 1665. [8] Lemelin et al. (2016) *Icarus*, under review. [9] Lucey, P. G. et al. (2000a) *JGR*, 105, 20297. [10] Lucey, P. G. et al. (2000b) *JGR*, 105, 20377. [11] Nelson, D. M. et al. (2014) *LPS*, 45, 2861. [12] McEwen, A. S. (1993) *JGR*, 98, 17207. [13] Hirata, N. et al. (2010) *LPS*, 41, 1585. [14] Gaddis, L. R. (1985) *Icarus*, 61, 461.